THE ASTROPHYSICAL JOURNAL, 448:70–83, 1995 July 20

A MULTIPARAMETRIC ANALYSIS OF THE *EINSTEIN* SAMPLE OF EARLY-TYPE GALAXIES. III. COMPARISONS WITH THE κ-PARAMETERS

PAUL B. ESKRIDGE[1]
Harvard-Smithsonian Center for Astrophysics; and Department of Physics and Astronomy,[2] University of Alabama, Tuscaloosa, AL 35487
GIUSEPPINA FABBIANO[1]
Harvard-Smithsonian Center for Astrophysics, 60 Garden Street, Cambridge, MA 02138
AND
DONG-WOO KIM[1]
Harvard-Smithsonian Center for Astrophysics, 60 Garden Street, Cambridge, MA 02138;
and Department of Astronomy and Space Science, Chungnam National University
Received 1994 October 10; accepted 1995 January 30

ABSTRACT

We have extended our bivariate and multivariate statistical analysis of the *Einstein* sample of early-type galaxies (Fabbiano, Kim, & Trinchieri 1992; Eskridge, Fabbiano, & Kim 1995a, b) to include a consideration of the κ-parameters defined by Bender, Burstein, & Faber (1992). The κ-parameters are defined such that κ_1 scales with virial mass, κ_3 scales with inner M/L ratio, and κ_2 is perpendicular to both κ_1 and κ_3. The κ_1-κ_3 plane is essentially edge-on to the Bender et al. (1992) formulation of the fundamental plane, and the parameter $\delta\kappa_3$ describes the scatter about that plane. We find that L_B, L_X, and L_6 are all strongly correlated with κ_1. Partial Spearman rank analysis shows these trends to be independent of the correlations between the luminosities. There are also significant bivariate trends of both L_X and L_6 with κ_3. Partial Spearman rank analysis indicates that the L_X-κ_3 trend is the dominant one, thus arguing for a connection between the prominence of X-ray coronae and the inner M/L. This suggests that galaxies with central excesses of dark matter also have more massive extended dark matter halos, providing a mechanism for retaining larger amounts of hot interstellar medium. We find evidence for a correlation between Mg_2 and $\delta\kappa_3$ that is independent of correlations of these two parameters with σ_v and is enhanced when tested for constant a_4. The strengthening of the Mg_2-$\delta\kappa_3$ correlation when tested for contant a_4 indicates an underlying connection between the scatter about the fundamental plane and the Type II supernova enrichment history of the central regions of elliptical galaxies that is independent of the details of the central structure of individual galaxies. This suggests that the Mg_2-$\delta\kappa_3$ trend is not related to the Mg_2 enhancements associated with kinematically decoupled cores seen in some disky elliptical galaxies (e.g., Bender & Surma 1992). It may be that systems with higher inner M/L_e (at a given mass) were more able to retain the metals generated in early epochs of star formation. Alternatively, systems experiencing more active or prolonged star formation may have produced an excess of baryonic dark matter from stellar remnants that is reflected in their higher M/L_e.

Subject headings: galaxies: elliptical and lenticular, cD — galaxies: ISM — X-rays: galaxies

1. INTRODUCTION

The *Einstein* sample of early-type galaxies (Fabbiano, Kim, & Trinchieri 1992, hereafter P0) is the largest currently available sample of E and S0 galaxies observed in X-rays. There are *Einstein* observations of 148 normal or nearly normal early-type galaxies in the sample. We have used this sample to explore the relationships of X-ray properties of E/S0 galaxies to other tracers of the insterstellar medium (ISM) (Eskridge, Fabbiano, & Kim 1995b, hereafter P1) and to observables related to the structure and stellar populations of the sample (Eskridge, Fabbiano, & Kim 1995a, hereafter P2). X-ray emission from luminous early-type galaxies is largely due to halos of gravitationally bound, hot ($T \sim 10^{6-7}$ K) gas (Forman et al. 1979; Forman, Jones, & Tucker 1985; Trinchieri & Fabbiano 1985). Such gas is often the dominant mass phase of the ISM in early-type galaxies (e.g., Fabbiano 1989, and references therein). Thus the *Einstein* sample offers us the opportunity to explore the physical relationships that govern the ISM, and to search for interrelationships between the ISM and other global properties of early-type galaxies.

In P1 we presented an analysis of the ISM properties of the *Einstein* sample. The major results of P1 are as follows: We confirm the results of earlier studies (see Fabbiano 1989, and references therein), finding a strong correlation between L_B and L_X, with a power-law slope of 1.8 ± 0.1. However, this is actually a combination of a slope-1 relation for the fainter galaxies ($\log L_X \leq 40.5$) and a slope-2 relation for the more luminous galaxies. This is consistent with other work indicating that X-ray–luminous early-type galaxies are so due to extensive halos of coronal gas, while X-ray–faint early-type galaxies owe their emission to unresolved stellar X-ray sources (e.g., Trinchieri & Fabbiano 1985; Fabbiano, Gioia, & Trinchieri 1989, hereafter FGT; Kim, Fabbiano, & Trinchieri 1992; Fabbiano, Kim, & Trinchieri 1994). The mean values of

[1] paul@hera.astr.ua.edu; pepi@cfa.harvard.edu; kim@cfa.harvard.edu.
[2] Current address.

the distribution functions of both L_X and L_X/L_B for the S0's are lower than those for the E's; thus, for a given stellar luminosity, the potential wells of S0's may be shallower than those of E's. Our S0 sample has excess 12 μm emission compared to the E's. This may be due to emission from dust heated in star-forming regions in S0 disks. This interpretation is supported by the existence of a strong L_{12}-L_{100} correlation for our S0 sample that is not found for the E's, and by an analysis of optical-IR colors. We also find strong indications of a connection between galaxy ISM and nuclear activity. There are steep power-law slopes between radio luminosity and optical, X-ray properties, and far-IR (FIR) properties. We note that, while L_B is most strongly correlated with L_6, the *total* radio luminosity (summed over a $\sim$1% bandwidth around 6 cm; see P1), both L_X and L_X/L_B are more strongly correlated with L_{6co}, the *core* radio luminosity. These points support the argument (proposed by FGT) that radio cores in early-type galaxies are fueled by the accretion of cooling flow gas from the hot ISM.

The picture that emerges from P1 connects the properties of the ISM in E and S0 galaxies to their star formation history and nuclear activity. In P2, we examined the structural and chemical properties of the sample, and how these relate to the hot ISM. The major results of P2 are as follows: Rounder and boxier galaxies tend to have larger L_X, L_X/L_B, and L_6 (the L_X-a_4 trend has been noted previously from smaller samples by Bender et al. 1989 and Djorgovski & de Carvalho 1990b). This suggests a connection between the shape of the potential and the ability to retain substantial halos of coronal gas. These in turn could be responsible for both feeding the nuclear sources through cooling flows and confining radio lobes (see also FGT). Both a/b and a_4 (the amplitude of the cos 4θ term of the Fourier decomposition of the shape of a galaxy's isophotes, following Bender et al. 1989) are correlated with L_B, but are not strongly correlated with either L_{12} or L_{100}. The lack of a trend with L_{12}, and the results of P1, indicates that there may be some significant contribution to the 12 μm emission from hot dust in early-type galaxies that is not directly related to the stellar component. For the S0's, there may be a contribution from dust associated with disk star formation regions.

There are strong correlations between Mg_2, σ_v, and L_X. Partial-rank analysis (see P1, and § 2 below) shows that the depth of the gravitational potential well (as measured by σ_v) is the crucial parameter. From a physical standpoint, the deeper the potential well, the better a galaxy is able to retain its hot ISM at the current epoch, and the better it was able to retain the enriched ejecta from its initial phase of strong star formation and reprocess this ejecta into new stars. We find a threshold of $\log \sigma_v \approx 2.2$ above which the maximum radio luminosities in our sample jump abruptly by more than an order of magnitude. Below this value of σ_v, it appears that the potential well is too shallow to efficiently transport material to the nuclear engine. It does not seem coincidental that, at this same value of σ_v, we see a jump in the maximum detected L_X/L_B of more than one order of magnitude.

Finally, X-ray, radio, and optical luminosities are all correlated with both shape (a/b and a_4) and depth (Mg_2 and σ_v) parameters. There are also strong relationships among the shape and the depth parameters. However, trends between the shape parameters (a/b and a_4) and one of the depth parameters (Mg_2 or σ_v) are modulated by the other parameter. That is, for instance, at a given a_4 value, the spread in σ_v appears directly related to the spread in Mg_2 such that the higher σ_v objects also have higher Mg_2. Alternatively, for a given σ_v, boxy galaxies tend to have *lower* Mg_2 values (and thus, we surmise, lower stellar abundances) than disky galaxies. This suggests that the presence of a hot ISM is dependent on both the shape (a/b, a_4) and the depth (Mg_2, σ_v) of the potential, but that these two families of parameters are not related in a simple way. These results, and the recent papers of Bender, Burstein, & Faber (1992, 1993), prompted us to search for relationships between the observables in our database and the κ-parameters defined by Bender et al. (1992).

The recent work of Bender et al. (1992, 1993) introduced a set of parameters (the κ-parameters) that provide an orthogonal coordinate system claimed to be a nearly perfect means of describing the "fundamental plane" of elliptical galaxies. This is a roughly planar, two-dimensional structure in the parameter space defined by central velocity dispersion, effective radius, and effective surface brightness, about which the properties of elliptical galaxies are seen to scatter. The existence of the fundamental plane was first pointed out by Dressler et al. (1987) and Djorgovski & Davis (1987; see Djorgovski & de Carvalho 1990a for a review). Bender et al. (1992) define the κ-parameters as follows:

$$\kappa_1 \equiv (\log \sigma_v^2 + \log r_e)/\sqrt{2}\,, \tag{1a}$$

$$\kappa_2 \equiv (\log \sigma_v^2 + 2 \log I_e - \log r_e)/\sqrt{6}\,, \tag{1b}$$

$$\kappa_3 \equiv (\log \sigma_v^2 - \log I_e - \log r_e)/\sqrt{3}\,. \tag{1c}$$

They also define the auxiliary parameter

$$\delta\kappa_3 \equiv \kappa_3 - 0.15\kappa_1 - 0.36\,. \tag{1d}$$

Here r_e is the effective radius, σ_v the central velocity dispersion, and I_e a measure of the effective surface brightness (see Bender et al. 1992 for details). Accepting the arguments of Bender et al. (1992), these definitions result in $\kappa_1 \propto \log M$, $\kappa_2 \propto \log (I_e^3 M/L_e)$, and $\kappa_3 \propto \log (M/L_e)$, where M/L_e is the mass-to-light ratio defined by a hybrid of central and effective radius properties and thus pertains to the inner part of the galaxy. The relationship $\kappa_3 - 0.15\kappa_1 - 0.36 = 0$ is their solution for the fundamental plane, thus the κ_1-κ_2 plane gives close to a face-on view of the fundamental plane, the κ_1-κ_3 plane gives an edge-on view, and $\delta\kappa_3$ measures the scatter about the fundamental plane. A comparison of X-ray data with the κ-parameters gives us another way to probe the link between emission properties (and thus the state of the ISM in early-type galaxies) and fundamental physical properties such as total mass and dark matter content.

The rest of the paper is organized as follows: In § 2 we discuss the nature and construction of our sample and briefly review our statistical methods. The results are given in § 3; trends with L_B in § 3.1, those with L_X in § 3.2, those with the 6 cm radio continuum properties in § 3.3, and those with *IRAS* 12 and 100 μm luminosities in § 3.4. Trends with structural and stellar properties of the sample are presented in §§ 3.5 and 3.6. In § 4 we review our results and suggest stratagies for future research. Some of the detailed statistical results are presented in the Appendix.

2. SAMPLE CONSTRUCTION AND ANALYSIS TECHNIQUES

There are 46 galaxies in common between the *Einstein* and Bender et al. (1992) samples. Table 1 gives the κ-parameter data for these objects. Other data used below can be found in Table 1 of P1 (axial ratio, and optical, X-ray, *IRAS*, and radio

TABLE 1

κ-PARAMETER DATA

Name	Type	κ_1	κ_2	κ_3	$\delta\kappa_3$
NGC 205	−3	2.219	2.898	0.856	0.163
NGC 221	−6	2.022	4.773	0.742	0.079
NGC 315	−3	4.652	2.988	1.010	−0.047
NGC 584	−2	3.818	3.756	0.766	−0.167
NGC 720	−5	3.977	3.525	0.924	−0.033
NGC 1052.....	−3	3.783	3.518	0.893	−0.034
NGC 1395.....	−5	4.003	3.517	0.968	0.007
NGC 1399.....	−5	4.045	3.798	0.991	0.025
NGC 1404.....	−5	3.708	3.982	0.795	−0.121
NGC 1407.....	−5	4.209	3.262	1.044	0.053
NGC 1553.....	−2	3.400	4.214	0.582	−0.288
NGC 1600.....	−5	4.506	3.069	0.993	−0.043
NGC 2300.....	−5	4.077	3.408	1.016	0.014
NGC 2694.....	−5	3.156	4.117	0.763	−0.070
NGC 2974.....	−5	3.880	3.460	0.929	−0.013
NGC 3115.....	−2	3.446	4.204	0.921	0.044
NGC 3377.....	−5	3.234	3.627	0.805	−0.040
NGC 3379.....	−5	3.509	3.970	0.874	−0.012
NGC 3607.....	−2	3.963	3.383	1.048	0.064
NGC 3608.....	−5	3.654	3.489	1.061	0.152
NGC 3818.....	−5	3.575	3.613	1.084	0.187
NGC 4168.....	−5	3.893	3.000	0.937	−0.007
NGC 4261.....	−5	4.120	3.531	1.009	0.031
NGC 4291.....	−5	3.710	4.004	0.985	0.068
NGC 4365.....	−5	3.918	3.471	1.042	0.094
NGC 4374.....	−5	4.002	3.726	0.980	0.019
NGC 4387.....	−5	2.855	3.516	0.676	−0.112
NGC 4406.....	−3	4.066	3.316	0.983	0.013
NGC 4467.....	−5	2.571	3.216	0.903	0.157
NGC 4472.....	−3	4.194	3.423	0.960	−0.029
NGC 4473.....	−5	3.469	3.897	0.792	−0.089
NGC 4551.....	−5	3.006	3.506	0.765	−0.046
NGC 4564.....	−5	3.332	3.722	0.857	−0.003
NGC 4589.....	−5	3.914	3.290	0.960	0.013
NGC 4621.....	−5	3.844	3.636	0.971	0.034
NGC 4636.....	−3	3.931	3.014	0.957	0.008
NGC 4649.....	−2	4.200	3.639	1.058	0.038
NGC 4697.....	−5	3.757	3.280	0.764	−0.159
IC 4296	−5	4.458	3.134	1.016	−0.013
NGC 5322.....	−5	3.933	3.586	0.789	−0.161
NGC 5576.....	−5	3.537	3.896	0.784	−0.107
NGC 5846.....	−2	4.242	3.094	1.084	0.058
NGC 7332.....	−2	3.020	4.577	0.445	0.368
IC 1459	−5	4.082	3.729	0.984	0.012
NGC 7619.....	−5	4.330	3.416	1.040	0.030
NGC 7626.....	−5	4.155	3.146	0.894	−0.089

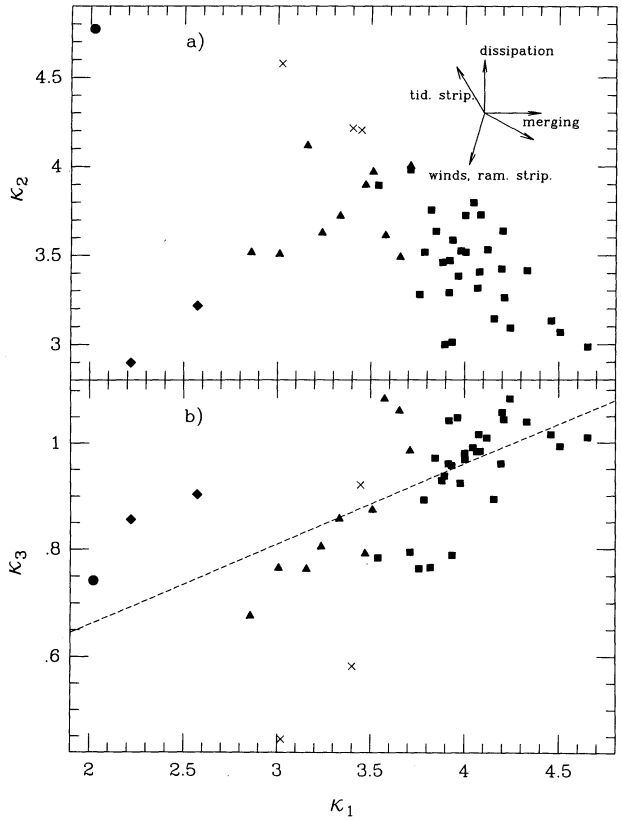

FIG. 1.—κ_1 vs. (*a*) κ_2 and (*b*) κ_3. Symbols are coded as in Bender et al. (1992): squares are giant ellipticals, triangles are intermediate ellipticals, diamonds are dwarf ellipticals, and crosses are S0 bulges; M32, a compact dE is shown as a solid circle. The arrows in (*a*) are from Bender et al. (1992) and show the directions that various processes will move objects in the κ_1-κ_2 plane. The dashed line in (*b*) shows the equation of the fundamental plane from Bender et al. (1992).

flux data) and Table 1 of P2 (Mg_2, σ_v, and a_4 measurements). In Figure 1 we show the κ_1-κ_2 and κ_1-κ_3 distributions of these galaxies, using the symbol conventions of Bender et al. (1992). We also include arrows in Figure 1*a* that indicate the directions that various physical processes will move galaxies in the κ_1-κ_2 plane following Bender et al. (1992). Our subsample of the Bender et al. (1992) galaxies is still large enough to outline the loci in the κ-planes and thus appears to be a fair sample. We note that the diffuse dwarfs NGC 205 and NGC 4467 are included in our sample. As these objects are structurally distinct from classical ellipticals (Kormendy 1985) we shall not include them in our analysis below. They shall, however, be included in the figures.

Many of our data in the X-ray, FIR, and radio are upper limits. Therefore, the use of standard statistical techniques is manifestly invalid for our project. Instead, we use techniques from the field of survival analysis for evaluating the existence of bivariate correlations among our data. These methods explicitly account for the existence of upper limits in the samples being tested, subject to regularity conditions that may or may not apply in the case of any given data sample. This last point is, of course, the standard problem in all astronomical statistical analysis. In an effort to minimize it, we use a number of different statistical tests, each with their own assumptions about the nature of the data and distribution of the upper limits, in the hopes that gross violations of the normality assumptions by our data will manifest themselves in highly discrepant results for the various statistical tests. Basic references in the astronomical literature for these methods are Feigelson & Nelson (1985), Schmitt (1985), Isobe, Feigelson, & Nelson (1986), La Valley, Isobe, & Feigelson (1992), and Feigelson & Babu (1992). Details of our particular procedures are given in P1.

As we are dealing with a multiparametric data set, it is important to investigate possible interrelationships between the various observables in our sample. A technique used in previous studies (Fabbiano, Gioia, & Trinchieri 1988; P1; P2) is the partial Spearman rank method (Kendall & Stuart 1976). In brief, to apply this method, one builds a matrix of modified Spearman rank coefficients for the parameters to be tested and then tests the correlation between subsamples of the parameters in the matrix set while holding all other variables in the matrix set constant. The major results of the partial-rank analysis are presented in the text below. The full details of our results are tabulated in the Appendix.

3. RESULTS

3.1. *Trends with* L_B

In Figure 2, we show plots of the κ-parameters against L_B. Table 2 shows the results of the bivariate correlation tests on these data. The strongest correlation is that between L_B and κ_1 ($P < 10^{-4}$; Fig. 2*a*). Weaker correlations are present between L_B and κ_2 (a negative trend at the $\lesssim$0.2% level), and with κ_3 (at the $\lesssim$0.7% level). Much of the scatter in the L_B-κ_2 and L_B-κ_3 plots (Figs. 2*b* and 2*c*, respectively) is caused by the few systems that are not "normal" ellipticals (the compact elliptical M32 and the bulges of S0 galaxies). We thus repeated the correlation analysis on subsets of the complete sample (see Table 2).

The negative correlation between L_B and κ_2 is significant for all tested samples. Recall that $\kappa_2 \propto I_e^3(M/L)$. Giant elliptical galaxies are known to show an anticorrelation between luminosity and surface brightness (L-Σ; e.g., Kormendy 1985). This result appears to reflect that trend and argues that the I_e^3 proportionality dominates that with M/L in κ_2 for giant ellipticals. The removal of the compact dE (M32) and the S0 bulges weakens the trend. This is in keeping with Kormendy's (1985) result that compact dE's and bulges are both known to follow the L-Σ relationship defined by giant ellipticals. The analysis shows almost perfect random scatter in the plot of L_B against $\delta\kappa_3$.

The L_B-κ_3 trend disappears if M32 is removed. Thus, we find no evidence for a relationship between optical luminosity and M/L_e for normal ellipticals. Given the range in L_B of our sample, this is completely in keeping with the results of Lauer (1985). We note that L_B and κ_3 both correlate with κ_1, but that the κ_1-κ_3 trend (the equation of the fundamental plane from Bender et al. 1992) has a very shallow slope (0.15). If there is such a shallow relation between L_B and κ_3, it could easily be masked by the scatter in our sample.

In Figure 3, we again show the distribution of our points in the κ-planes, but using different symbols for quartiles in L_B. We note that the most optically luminous galaxies tend to cluster in the "merging corner" of Bender et al. (1992), and that the distribution of points is generally as expected from the definitions of the κ-parameters.

3.2. *Trends with* L_X

Plots of the κ-parameters against L_X are shown in Figure 4. Results of the bivariate correlation tests are given in Table 2. As for L_B, there is an obvious trend between κ_1 and L_X. The strength of this trend is essentially unaffected by removing M32 and the S0 bulges. Partial-rank analysis shows that the L_X-κ_1 relationship is weaker than that between L_B and κ_1, but is still significant when taken for constant L_B (see Table A1). Therefore there is a direct link between mass and the presence of a hot ISM. This agrees with previous results (FGT; P1; P2) and with model predictions (e.g., Ciotti et al. 1991). We also find a statistically significant negative bivariate correlation between κ_2 and L_X. However, partial-rank analysis shows the L_X-κ_2 trend to be driven by mutual correlations with L_B.

A stronger correlation (at the less than 0.4% level in all tests) exists between κ_3 with L_X. This correlation is confirmed by partial-rank analysis at the $\sim$1.5% level, while no trend is found between L_B and κ_3 (see Table A3). This result can also be seen by an examination of the κ-planes using quartiles in L_X (Fig. 5): the highest L_X galaxies are much more tightly clustered in the upper-right corner of the κ_1-κ_3 plane than are the highest L_B galaxies (see Fig. 3). The difference between Figures 3 and 5 appears entirely due to the correlation of κ_3 with L_X. More X-ray–luminous galaxies tend to have higher M/L_e. The same is not true for optically luminous galaxies. Figure 5 also shows that high-L_X galaxies are not especially more concentrated in the merging corner of the κ_1-κ_2 plane, (while Fig. 3 does show such a concentration for the high-L_B galaxies), so merging is not necessarily a key factor in producing high-L_X galaxies. This is contrary to the early conclusions of Bender et al. (1989; see also Djorgovski & de Carvalho 1990a).

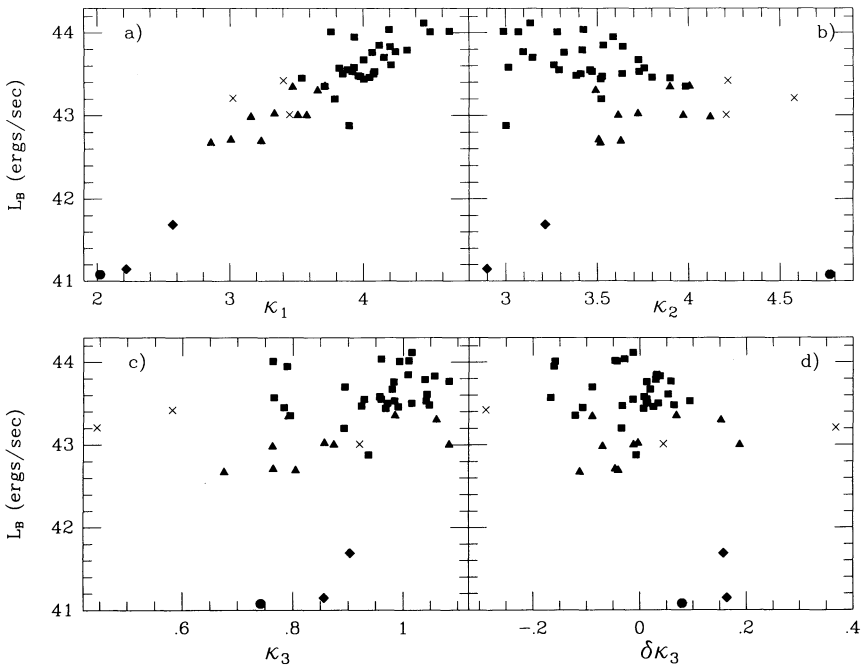

FIG. 2.—κ-parameters vs. L_B. Symbols as in Fig. 1.

TABLE 2A

BIVARIATE CORRELATION TESTS WITH THE LUMINOSITY PARAMETERS

PARAMETER	κ_1		κ_2		κ_3		$\delta\kappa_3$	
	N_{tot}[a]	N_{lim}[b]	N_{tot}[a]	N_{lim}[b]	N_{tot}[a]	N_{lim}[b]	N_{tot}[a]	N_{lim}[b]
L_B	44	0	44	0	44	0	44	0
	63.213	$<10^{-4}$	10.002	0.0016	7.309	0.0069	1.403	0.2363
	6.313	$<10^{-4}$	3.845	0.0001	2.945	0.0032	0.395	0.6931
	0.843	$<10^{-4}$	−0.540	0.0004	0.445	0.0035	−0.075	0.6245
L_X	44	14	44	14	44	14	44	14
	23.415	$<10^{-4}$	9.294	0.0023	9.941	0.0016	0.178	0.6732
	5.528	$<10^{-4}$	2.990	0.0028	3.496	0.0005	0.376	0.7066
	0.798	$<10^{-4}$	−0.452	0.0030	0.529	0.0005	0.057	0.7061
L_X/L_B	44	14	44	14	44	14	44	14
	16.870	$<10^{-4}$	8.860	0.0029	8.957	0.0028	0.057	0.8109
	4.597	$<10^{-4}$	2.767	0.0057	3.203	0.0014	0.257	0.7974
	0.679	$<10^{-4}$	−0.411	0.0070	0.483	0.0015	0.054	0.7218
L_{12}	41	16	41	16	41	16	41	16
	11.426	0.0007	2.788	0.0950	3.075	0.0795	0.021	0.8859
	3.002	0.0027	1.309	0.1904	1.948	0.0514	0.287	0.7738
	0.445	0.0049	−0.170	0.2835	0.312	0.0483	0.033	0.8345
L_{100}	41	16	41	16	41	16	41	16
	10.501	0.0012	5.622	0.0177	0.714	0.3980	1.122	0.2894
	3.254	0.0011	2.478	0.0132	1.477	0.1396	1.277	0.2016
	0.520	0.0010	−0.398	0.0118	0.247	0.1189	−0.199	0.2084
L_6	44	19	44	19	44	19	44	19
	20.435	$<10^{-4}$	11.511	0.0007	10.582	0.0011	0.243	0.6220
	5.127	$<10^{-4}$	2.974	0.0029	2.852	0.0043	0.100	0.9204
	0.749	$<10^{-4}$	−0.459	0.0026	0.450	0.0031	0.030	0.8455

NOTE.—The diffuse dE's NGC 205 and NGC 4467 are not included.

[a] Values in rows 2–4 of each entry are the test scores for the Cox-Hazard, Kendall's τ, and Spearman rank correlation tests, respectively.

[b] Values in rows 2–4 of each entry are probabilities for the corresponding correlation test.

TABLE 2B

BIVARIATE CORRELATION TESTS WITH THE LUMINOSITY PARAMETERS

PARAMETER	κ_1		κ_2		κ_3		$\delta\kappa_3$	
	N_{tot}	N_{lim}	N_{tot}	N_{lim}	N_{tot}	N_{lim}	N_{tot}	N_{lim}
L_B	43	0	43	0	43	0	43	0
	47.562	$<10^{-4}$	8.478	0.0036	3.413	0.0647	0.556	0.4559
	6.082	$<10^{-4}$	3.528	0.0004	2.660	0.0078	0.042	0.9666
	0.831	$<10^{-4}$	−0.507	0.0010	0.409	0.0080	−0.017	0.9139
L_X	43	14	43	14	43	14	43	14
	29.475	$<10^{-4}$	7.841	0.0051	8.479	0.0036	0.059	0.8080
	5.383	$<10^{-4}$	2.764	0.0057	3.308	0.0009	0.666	0.5054
	0.793	$<10^{-4}$	−0.432	0.0051	0.504	0.0011	0.086	0.5783
L_X/L_B	43	14	43	14	43	14	43	14
	20.307	$<10^{-4}$	7.090	0.0078	7.218	0.0072	0.001	0.9794
	4.416	$<10^{-4}$	2.525	0.0116	2.998	0.0027	0.553	0.5799
	0.649	$<10^{-4}$	−0.369	0.0167	0.442	0.0042	0.088	0.5702
L_{12}	40	16	40	16	40	16	40	16
	9.881	0.0017	0.519	0.4711	1.937	0.1639	0.078	0.7805
	2.726	0.0064	0.964	0.3350	1.696	0.0899	0.632	0.5276
	0.415	0.0096	−0.122	0.4447	0.274	0.0870	0.101	0.5265
L_{100}	40	15	40	15	40	15	40	15
	10.500	0.0012	3.721	0.0537	0.298	0.5853	0.616	0.4326
	3.042	0.0023	2.239	0.0251	1.256	0.2092	1.049	0.2943
	0.488	0.0023	−0.360	0.0246	0.204	0.2017	−0.145	0.3642
L_6	43	18	43	18	43	18	43	18
	25.775	$<10^{-4}$	11.062	0.0009	9.209	0.0024	0.463	0.4962
	5.001	$<10^{-4}$	2.781	0.0054	2.656	0.0079	0.366	0.7141
	0.731	$<10^{-4}$	−0.419	0.0067	0.417	0.0069	0.090	0.5583

NOTES.—The compact dE M32 has been removed. Table entries as defined in notes to Table 2A.

TABLE 2C

BIVARIATE CORRELATION TESTS WITH THE LUMINOSITY PARAMETERS

PARAMETER	κ_1		κ_2		κ_3		$\delta\kappa_3$	
	N_{tot}	N_{lim}	N_{tot}	N_{lim}	N_{tot}	N_{lim}	N_{tot}	N_{lim}
L_B	40	0	40	0	40	0	40	0
	45.665	$<10^{-4}$	7.080	0.0078	2.619	0.1056	0.124	0.7243
	5.828	$<10^{-4}$	3.217	0.0013	2.343	0.0191	0.245	0.8066
	0.818	$<10^{-4}$	−0.477	0.0029	0.365	0.0227	0.022	0.8905
L_X	40	12	40	12	40	12	40	12
	26.219	$<10^{-4}$	6.045	0.0139	10.280	0.0013	0.759	0.3835
	5.128	$<10^{-4}$	2.324	0.0201	3.050	0.0023	1.181	0.2377
	0.789	$<10^{-4}$	−0.372	0.0201	0.487	0.0024	0.190	0.2343
L_X/L_B	40	12	40	12	40	12	40	12
	17.951	$<10^{-4}$	5.818	0.0159	8.852	0.0029	1.379	0.2402
	4.148	$<10^{-4}$	2.100	0.0358	2.753	0.0059	1.114	0.2653
	0.628	0.0001	−0.306	0.0557	0.418	0.0090	0.193	0.2282
L_{12}	37	16	37	16	37	16	37	16
	8.401	0.0038	0.230	0.6312	3.992	0.0457	0.247	0.6188
	2.179	0.0293	0.436	0.6630	1.459	0.1444	0.967	0.3337
	0.354	0.0338	−0.034	0.8401	0.241	0.1477	0.145	0.3834
L_{100}	37	14	37	14	37	14	37	14
	11.896	0.0006	5.332	0.0209	1.785	0.1815	0.534	0.4650
	2.951	0.0032	2.195	0.0282	1.265	0.2059	0.712	0.4762
	0.501	0.0027	−0.370	0.0265	0.225	0.1767	−0.082	0.6207
L_6	40	15	40	15	40	15	40	15
	22.746	$<10^{-4}$	8.676	0.0032	8.852	0.0029	0.915	0.3389
	4.730	$<10^{-4}$	2.322	0.0203	2.285	0.0223	0.546	0.5848
	0.721	$<10^{-4}$	−0.359	0.0250	0.389	0.0150	0.140	0.3828

NOTES.—M32 and the S0 bulges (NGC 1553, NGC 3115, and NGC 7332) removed. Table entries as defined in notes to Table 2A.

The L_X-κ_3 correlation points to a relationship between a global property of elliptical galaxies (the amount of hot ISM they are able to retain) and a property of the cores of elliptical galaxies (their inner M/L ratios). If the depth of the gravitational potential is a major factor in the ability of galaxies to retain their hot ISM (see, e.g., Ciotti et al. 1991), the L_X-κ_3 relationship we find suggests that galaxies with relatively larger amounts of dark matter in their inner regions tend to have more massive dark matter halos.

As a number of parameters considered in earlier parts of this study (see P1 and P2) correlate more strongly with L_X/L_B than with either L_B or L_X, we examined the relationship of the κ-parameters against L_X/L_B. No interesting correlations were found. The results of the statistical analysis are shown in Table 2.

3.3. *Trends with the* 6 cm *Radio Luminosity*

We find a very strong correlation between κ_1 and L_6 (nearly as strong as that with L_X) for all the samples we test (see Fig. 6 and Table 2). Inspection of Figure 6*a* shows a threshold, as for other trends with L_6 discussed in P2: All systems detected at 6 cm have $\kappa_1 \geq 3.5$. There is a significant negative trend between κ_2 and L_6 for all tested samples. There is also a significant trend between κ_3 and L_6 for all tested samples, in the sense that those systems with the largest M/L_e ratios have the strongest nonthermal radio emission. In keeping with this, we find that, as for L_X, the most radio-luminous galaxies in our sample are tightly clustered in the upper-right corner of the κ_1-κ_3 plane (see Fig. 7).

Partial-rank analysis, including L_6 along with L_B, L_X, and the κ-parameters, shows that the bivariate trends of L_6 with κ_2 and κ_3 are likely to be driven by underlying relationships of L_6, κ_2, and κ_3 with both L_B and L_X. However, the strong bivariate L_6-κ_1 trend is maintained when L_B and L_X dependencies are considered. Thus we find a strong relationship between the virial mass of early-type galaxies and their ability to generate nonthermal radio power. This relationship is *independent* of trends with either optical or X-ray luminosity.

3.4. *Trends with Mid-IR and FIR Luminosities*

Table 2 shows that the only significant correlation including L_{12} is that with κ_1. It is, however, much weaker than the correlations between κ_1 and L_B, L_X, or L_6. Also, when one considers only giant and intermediate ellipticals (see Table 2C), the correlation is marginal at best. There are no significant trends with any of the other κ-parameters.

The correlation between κ_1 and L_{100} is stronger than that between κ_1 and L_{12} and is significant for all of the samples tested. There is also a significant negative correlation (at the 1%–2% level) between κ_2 and L_{100}. However, a partial-rank analysis on L_B, L_{100}, L_6, and the κ-parameters indicates that the L_{100} trends found here are driven by the L_{100}-L_6 and L_B-L_{100} relationships found in P1, and the L_6-κ trends discussed in § 3.3 above.

3.5. *Trends with the Shape Parameters* a/b and a_4

Table 3 shows some evidence for trends between κ_1, κ_3, and a/b, in the sense that larger κ_1 or κ_3 trends to imply rounder isophotes. This is reminiscent of the results presented in P2. Partial-rank analysis indicates that these trends are driven by the underlying trend of a/b with σ_v (see P2, and Table A3). There is no compelling evidence for trends of a/b with either κ_2 or $\delta\kappa_3$. Similarly, we find no significant correlations of a_4 with any of the κ-parameters. Our results are in agreement with

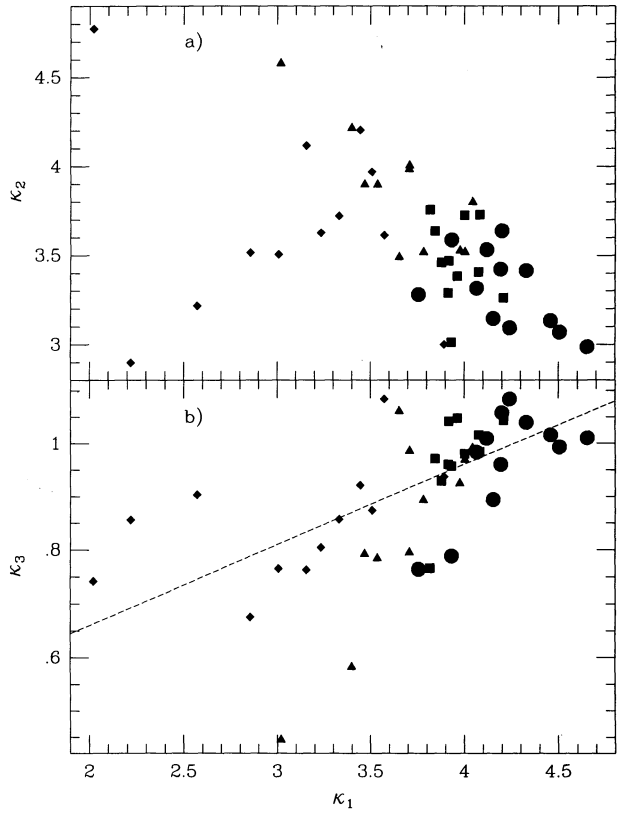

FIG. 3.—κ_1 vs. (*a*) κ_2 and (*b*) κ_3. Symbols are coded in quartiles of L_B, with the solid circles being the most optically luminous galaxies, then the squares, then the triangles. The diamonds are the optically faintest galaxies in our sample.

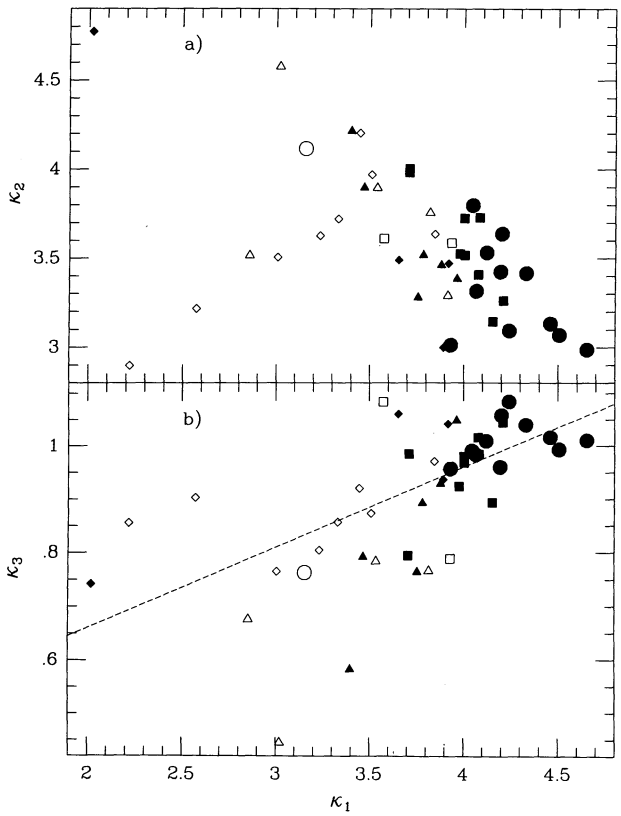

FIG. 5.—κ_1 vs. (*a*) κ_2 and (*b*) κ_3. Symbols are coded as in Fig. 3, but in quartiles of L_X, with open symbols for systems with upper limits in L_X.

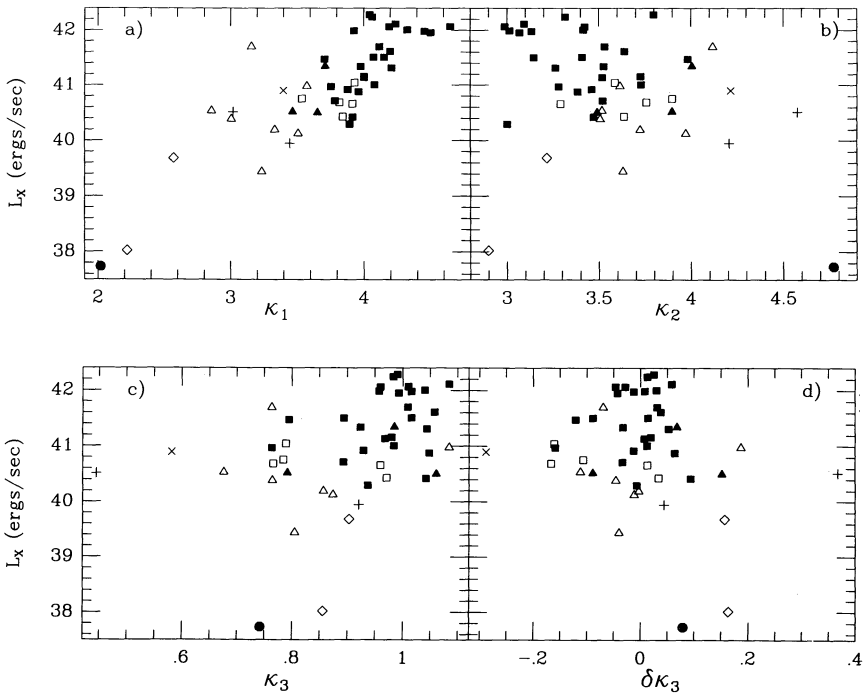

FIG. 4.—κ-parameters vs. L_X. Symbols as in Fig. 1 for X-ray detections. Open symbols for X-ray upper limits (plus signs for X-ray upper limits on S0 bulges).

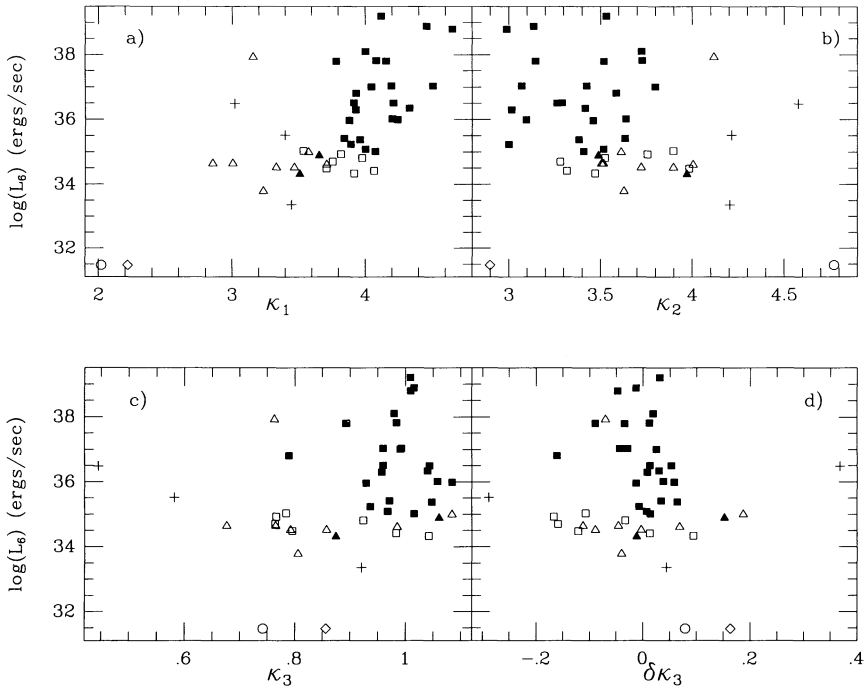

FIG. 6.—κ-parameters vs. L_6. Symbols as in Fig. 4.

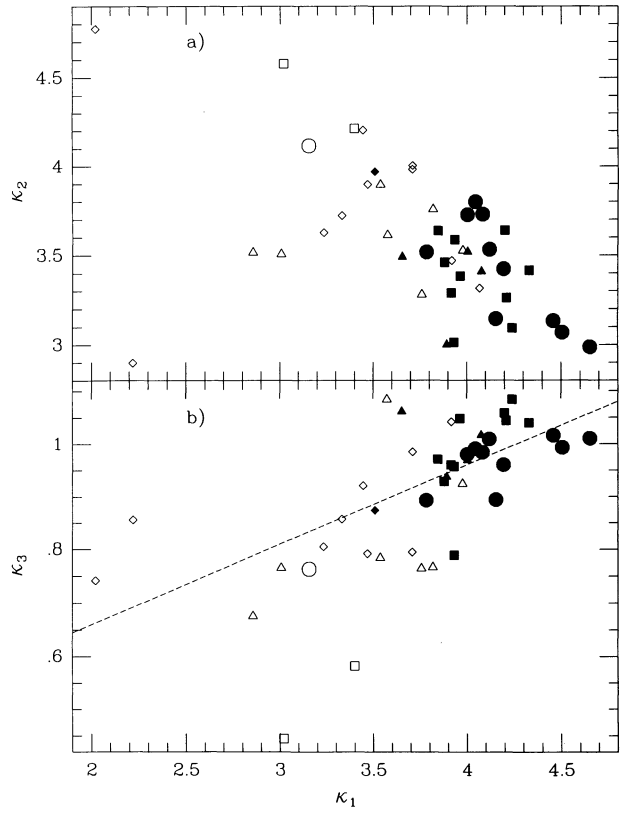

FIG. 7.—κ_1 vs. (*a*) κ_2 and (*b*) κ_3. Symbols are coded as in Fig. 5, but in quartiles of L_6, with open symbols for systems with upper limits in L_6.

previous conclusions pointing to a lack of correlation between axial ratio and the fundamental properties of early-type galaxies (e.g., Vader 1986).

3.6. *Trends with* Mg_2 *and* σ_v

Given the definition of κ_1 and κ_3, strong bivariate correlations are expected (and found) with σ_v irrespective of sample. Bivariate correlations are also found between Mg_2 and both κ_1 and κ_3 (see Table 3 and Fig. 8). However, partial-rank analysis shows that these are driven by the underlying strong Mg_2-σ_v trend (see Tables A1 and A3; see also Bender et al. 1993; P2). We find no evidence for any trend between κ_2 and either σ_v or Mg_2.

We find evidence for a positive trend between σ_v and $\delta\kappa_3$ for samples with the dwarf galaxies removed from our bivariate analysis (see Tables 3B and 3C and Fig. 9). A stronger bivariate correlation exists between Mg_2 and $\delta\kappa_3$ once we remove M32 from the sample (see Tables 3B and 3C and Fig. 8). The results of the partial-rank analysis indicate that the Mg_2-$\delta\kappa_3$ and Mg_2-σ_v trends are what drives the bivariate σ_v-$\delta\kappa_3$ correlation (see Table A4). This is important, as one could otherwise argue for a weak residual dependance of $\delta\kappa_3$ on σ_v on the basis of dimensional analysis. The inclusion of a_4 in the partial-rank analysis yields a *much* stronger correlation of Mg_2 with $\delta\kappa_3$, for a_4 constant. Analogous behavior is seen with a/b (the most interesting results are shown in Tables A1–A4).

As the Mg_2-$\delta\kappa_3$ trend is not due to underlying relationships of both these parameters with σ_v, we are forced to consider possible reasons for a $\delta\kappa_3$-Mg_2 correlation. The evolutionary pathway for enrichment of Mg (e.g., Woosley & Weaver 1986) indicates that the scatter about the fundamental plane may be associated with variation in the SN II rate from system to system, and thus with the differences in early epochs of star formation in different systems. It may be that the high-Mg_2 systems are merger products in which secondary central disks

TABLE 3A

BIVARIATE CORRELATIONS WITH THE STRUCTURAL AND STELLAR PARAMETERS

	κ_1		κ_2		κ_3		$\delta\kappa_3$	
PARAMETER	N_{tot}	N_{lim}	N_{tot}	N_{lim}	N_{tot}	N_{lim}	N_{tot}	N_{lim}
a/b	44	0	44	0	44	0	44	0
	8.399	0.0038	2.425	0.1194	4.482	0.0343	1.516	0.2183
	2.796	0.0052	1.398	0.1621	2.270	0.0232	0.942	0.3460
	−0.401	0.0085	0.198	0.1937	−0.341	0.0255	−0.140	0.3575
Mg_2	41	0	41	0	41	0	41	0
	13.324	0.0003	3.088	0.0789	24.464	$<10^{-4}$	0.354	0.5517
	3.946	0.0001	0.753	0.4513	3.868	0.0001	2.204	0.0275
	0.581	0.0002	−0.136	0.3910	0.582	0.0002	0.355	0.0248
σ_v	41	0	41	0	41	0	41	0
	73.744	$<10^{-4}$	2.486	0.1149	23.918	$<10^{-4}$	0.224	0.6363
	6.493	$<10^{-4}$	1.236	0.2166	5.000	$<10^{-4}$	1.719	0.0856
	0.861	$<10^{-4}$	−0.202	0.2010	0.704	$<10^{-4}$	0.290	0.0671
a_4	31	0	31	0	31	0	31	0
	5.822	0.0158	0.353	0.5526	$<10^{-3}$	0.9968	0.129	0.7199
	1.838	0.0661	0.374	0.7082	0.953	0.3407	0.017	0.9864
	−0.309	0.0902	0.099	0.5866	−0.135	0.4597	−0.012	0.9498

NOTES.—The diffuse dE's are not included. Table entries as defined in notes to Table 2A.

TABLE 3B

BIVARIATE CORRELATIONS WITH THE STRUCTURAL AND STELLAR PARAMETERS

	κ_1		κ_2		κ_3		$\delta\kappa_3$	
PARAMETER	N_{tot}	N_{lim}	N_{tot}	N_{lim}	N_{tot}	N_{lim}	N_{tot}	N_{lim}
a/b	43	0	43	0	43	0	43	0
	9.115	0.0025	4.465	0.0346	4.691	0.0303	1.493	0.2218
	2.925	0.0034	1.478	0.1394	2.317	0.0205	0.986	0.3243
	−0.424	0.0060	0.211	0.1708	−0.352	0.0224	−0.142	0.3568
Mg_2	40	0	40	0	40	0	40	0
	7.361	0.0067	0.022	0.8830	16.020	0.0001	11.951	0.0005
	3.627	0.0003	0.315	0.7529	3.569	0.0004	2.683	0.0073
	0.548	0.0006	−0.069	0.6661	0.550	0.0006	0.446	0.0053
σ_v	40	0	40	0	40	0	40	0
	64.654	$<10^{-4}$	0.012	0.9120	17.875	$<10^{-4}$	4.765	0.0290
	6.269	$<10^{-4}$	0.816	0.4147	4.744	$<10^{-4}$	2.179	0.0293
	0.850	$<10^{-4}$	−0.141	0.3792	0.681	$<10^{-4}$	0.380	0.0176

NOTES.—The compact dE M32 has been removed. Table entries as defined in notes to Table 2A.

TABLE 3C

BIVARIATE CORRELATIONS WITH THE STRUCTURAL AND STELLAR PARAMETERS

	κ_1		κ_2		κ_3		$\delta\kappa_3$	
PARAMETER	N_{tot}	N_{lim}	N_{tot}	N_{lim}	N_{tot}	N_{lim}	N_{tot}	N_{lim}
a/b	40	0	40	0	40	0	40	0
	3.304	0.0691	0.417	0.5184	1.483	0.2232	0.552	0.4574
	2.218	0.0266	0.467	0.6405	1.728	0.0840	1.670	0.0950
	−0.337	0.0352	0.054	0.7376	−0.274	0.0875	−0.266	0.0970
Mg_2	39	0	39	0	39	0	39	0
	7.466	0.0063	0.035	0.8513	15.892	0.0001	12.347	0.0004
	3.633	0.0003	0.242	0.8086	3.500	0.0005	2.798	0.0051
	0.554	0.0006	−0.053	0.7445	0.548	0.0007	0.468	0.0039
σ_v	39	0	39	0	39	0	39	0
	67.934	$<10^{-4}$	0.152	0.6962	17.908	$<10^{-4}$	4.631	0.0314
	6.570	$<10^{-4}$	1.004	0.3153	4.768	$<10^{-4}$	2.178	0.0294
	0.891	$<10^{-4}$	−0.169	0.2965	0.691	$<10^{-4}$	0.380	0.0192

NOTES.—M32 and the S0 bulges (NGC 1553, NGC 3115, and NGC 7332) have been removed. Table entries as defined in notes to Table 2A.

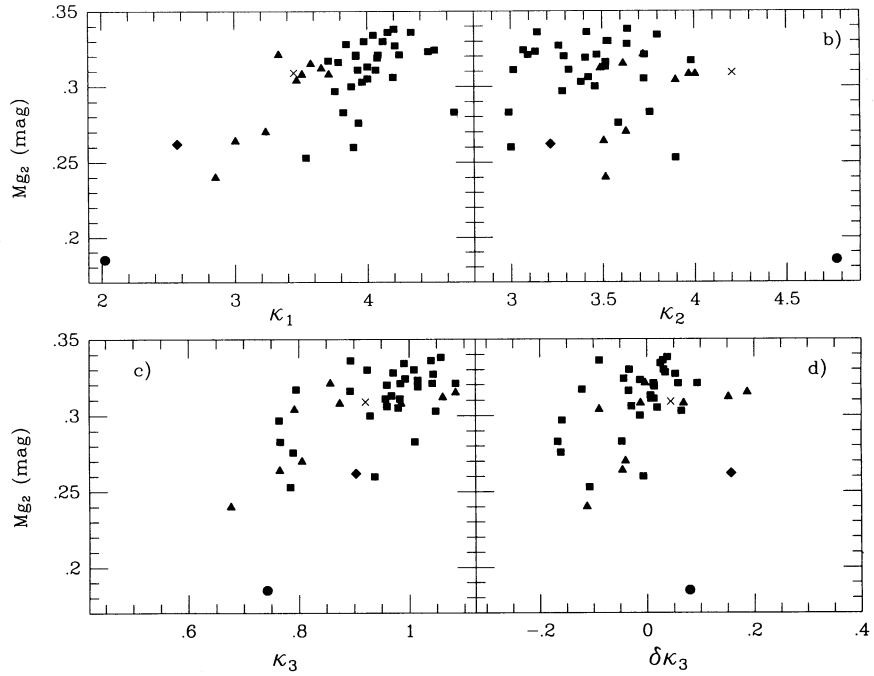

FIG. 8.—κ-parameters vs. Mg_2. Symbols as in Fig. 4.

have formed and undergone (now intermediate-age) bursts of star formation (Bender & Surma 1992; P2), although the strengthening of the Mg_2-$\delta\kappa_3$ trend for constant a_4 argues against this. Such a situation would cause a weakening of the Mg_2-$\delta\kappa_3$ correlation when tested for constant a_4, the opposite of what is observed.

The sense of the correlation indicates that systems with anomalously high M/L_e for their mass also tend to have enhanced Mg_2 values. These enhanced Mg_2 values may be due to an overall enhancement in metallicity in the cores of the affected galaxies. Thus it may simply be that those systems with higher M/L_e (at a given mass) were more able to retain the metals generated in early epochs of star formation (due to less effective galactic winds; see, e.g., Ciotti et al. 1991). Another possibility is that large (central) Mg_2 values reflect enhanced abundances of elements primarily produced in Type II supernovae. Galaxies with such enhancements may have experienced enhanced central star formation at some point and are thus also systems that have a significant fraction of baryonic dark matter in the form of stellar remnants. Our data do not allow

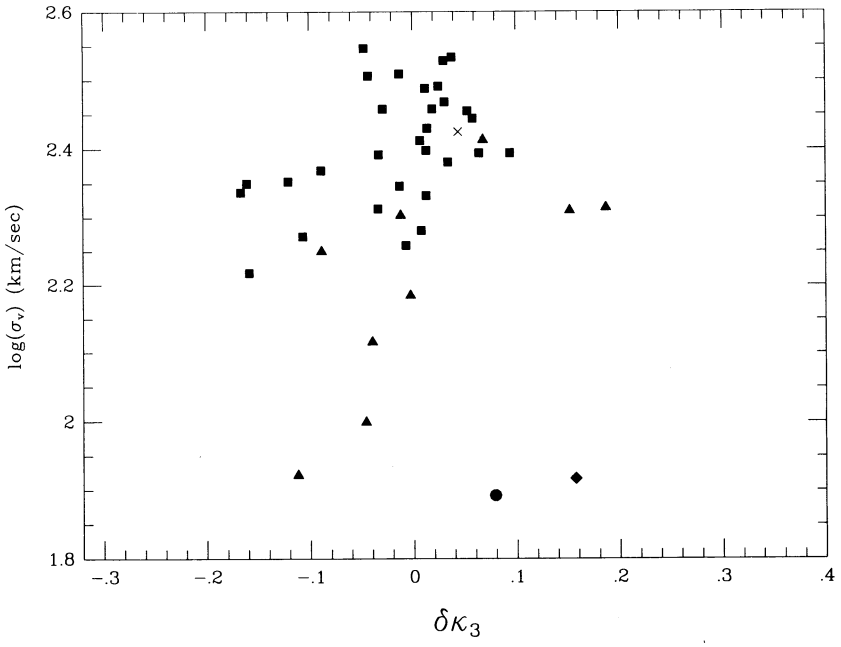

FIG. 9.—$\delta\kappa_3$ vs. log σ_v. Symbols as in Fig. 4.

us to distinguish among these alternatives, although a number of recent and ongoing studies are shedding further light on this area (e.g., Buzzoni, Gariboldi, & Mantegazza 1992; Worthey, Faber, & Gonzalez 1992; Carollo, Danziger, & Buson 1993; Davies, Sadler, & Peletier 1993; Worthey 1993).

4. SUMMARY AND SUGGESTIONS FOR FUTURE RESEARCH

The main results of this study are as follows:

1. There are strong bivariate correlations of κ_1 with L_B, L_X, and L_6, all of which are upheld in a partial-rank analysis. Of these, the strongest is that between κ_1 and L_B. However, the correlations between κ_1 and both L_X and L_6 are still significant for constant L_B. These correlations point to galaxy mass as a key factor in X-ray and radio emission. This agrees with previous results pointing to the galaxy potential as a key factor in the retention of a hot ISM (e.g., FGT; Ciotti et al. 1991; P1; P2) and linking nuclear accretion of the latter, through cooling flows, to nuclear activity (FGT).

2. There are strong bivariate correlations between κ_3 and both L_X and L_6. Also, the distribution of points in the κ_1-κ_3 plane shows a much tighter grouping among the X-ray– or radio-brightest galaxies than among the optically brightest galaxies. Partial-rank analysis demonstrates that the L_X-κ_3 relationship is the dominant one, and that this trend holds up at the $\sim$1.5% confidence level when tested for constant L_B. This argues for a connection between a global property of galaxies (the amount of material in their X-ray coronae) and a core property (the inner M/L). The current finding may thus fit into the general framework of the fueling of central sources by cooling X-ray gas as suggested by FGT. It also suggests that variations in dark matter content (at a given optical luminosity) among elliptical galaxies may be a crucial factor in determining whether they can retain halos of coronal X-ray gas, and that the relative excess of dark matter in the core is an index of the presence of larger dark matter halos. A similar connection was made in P1 between L_X and the core radio luminosity.

3. While high-L_B galaxies tend to concentrate in the "merging corner" of the κ_1-κ_2 diagram (see Bender et al. 1992), the same is not true for high-L_X galaxies. Merging, therefore, may not be a key factor for the presence of a hot ISM.

4. We find evidence for bivariate trends between $\delta\kappa_3$ and both Mg_2 and σ_v. Partial-rank analysis indicates that the Mg_2-$\delta\kappa_3$ trend is the fundamental one. This result does not appear to be caused by a residual definitional dependence of $\delta\kappa_3$ on σ_v. The sense of the trend is that systems that have high M/L_e for their mass also tend to have enhanced central Mg_2 values. This may be due to the enhanced ability of such galaxies to maintain ongoing or episodic central star formation for extended periods, or to retain the enriched ejecta of early epochs of star formation, or both. The Mg_2-$\delta\kappa_3$ trend becomes stronger when tested for constant a_4. This suggests that the Mg_2-$\delta\kappa_3$ correlation cannot be entirely driven by the existence of metal-rich nuclear disks (such as those discovered by Bender & Surma 1992) in systems that scatter above the fundamental plane. Were this so, the trend would become weaker, rather than stronger, when evaluated for constant a_4, as it would be due to an Mg_2 enhancement that is linked to the presence of disky isophotes.

These findings suggest a number of areas for future study. The connection between global properties and the inner M/L ratio may be due to an underlying similarity in the overall potential structures of early-type galaxies. In this case, those systems with the highest inner M/L ratio would also tend to have the highest global M/L ratios. Current work on *ROSAT* data of early-type galaxies may help to resolve this puzzle. The relationship of the metal abundance parameter Mg_2 with the scatter about the Bender et al. (1992) realization of the fundamental plane is also a finding that begs for future research. In particular, it is important to see if such a trend is upheld for the Fe lines as well as Mg_2. It would also be very interesting to see if there are any effects with either Mg_2 or Fe line radial gradients. Given current efforts (many referred to above) in optical spectroscopy of elliptical galaxies, both of these projects could be accomplished in the next few years.

We would like to thank David Burstein for suggesting that we consider the κ-parameters as part of our study, and George Djorgovski for refereeing the paper. We thank Glen Mackie and Ginevra Trinchieri for their comments on this study as it has progressed. We also thank Eric Feigelson and Michael LaValley for providing us with the lastest versions of the ASURV software package. G. F. would like to thank the Aspen Summer School for the opportunity to focus on this project. This research has made use of the NASA/IPAC Extragalactic Database (NED) which is operated by the Jet Propulsion Laboratory, Caltech, under contract with the National Aeronautics and Space Administration. We are grateful to the National Aeronautics and Space Administration for support of this research under the LTSA grant NAGW-2681 and contract NAS 8-39073 (AXAF Science Center).

APPENDIX

Tables A1–A4 contain the detailed results of the partial Spearman rank statistical analysis for those trends that are strong enough to warrant notice. Table A1 shows the analysis of trends with κ_1 (L_B, L_X, L_6, and Mg_2 are shown). Table A2 shows the analysis of trends with κ_2 (only L_B is shown). Table A3 shows the analysis of trends with κ_3 (L_B, L_X, a/b, and Mg_2 are shown). Table A4 shows the analysis of trends with $\delta\kappa_3$ (a/b, Mg_2, and σ_v are shown). Within each section, column (1) identifies the test pair and the quantities to be held constant in the test, column (2) gives the sample under consideration ("Full" means all available non-dE's are included, "No cE's" means that the compact dwarf M32 has been excluded, and "No S0's" means that the S0 bulges have *also* been excluded). Column (3) gives the number of objects in the sample. Column (4) gives the partial Spearman rank statistic. Column (5) gives the probability that the test pair are uncorrelated for that set of parameters.

TABLE A1

PARTIAL SPEARMAN RANK ANALYSIS: TRENDS WITH κ_1

Test Pair[a] and Held Parameters (1)	Sample (2)	Size (3)	Partial Spearman Rank (4)	Probability (5)
L_B-κ_1:				
L_X	Full	44	0.673	<0.005
L_X	No cE's	43	0.643	<0.005
L_X	No S0's	40	0.640	<0.005
L_6	Full	44	0.708	<0.005
L_6	No cE's	43	0.702	<0.005
L_6	No S0's	40	0.692	<0.005
L_X, L_6	Full	44	0.562	<0.005
L_X, L_6	No cE's	43	0.544	<0.005
L_X, L_6	No S0's	40	0.536	<0.005
L_X-κ_1:				
L_B	Full	44	0.560	<0.005
L_B	No cE's	43	0.544	<0.005
L_B	No S0's	40	0.572	<0.005
L_6	Full	44	0.701	<0.005
L_6	No cE's	43	0.690	<0.005
L_6	No S0's	40	0.710	<0.005
L_B, L_6	Full	44	0.550	<0.005
L_B, L_6	No cE's	43	0.523	<0.005
L_B, L_6	No S0's	40	0.567	<0.005
L_6-κ_1:				
L_B	Full	44	0.493	<0.005
L_B	No cE's	43	0.487	<0.005
L_B	No S0's	40	0.494	<0.005
L_X	Full	44	0.621	<0.005
L_X	No cE's	43	0.586	<0.005
L_X	No S0's	40	0.607	<0.005
L_B, L_X	Full	44	0.481	<0.005
L_B, L_X	No cE's	43	0.461	<0.005
L_B, L_X	No S0's	40	0.487	<0.005
Mg_2-κ_1:				
a/b	Full	41	0.488	<0.005
a/b	No cE's	40	0.434	<0.005
a/b	No S0's	39	0.449	<0.005
σ_v	Full	41	0.148	0.192
σ_v	No cE's	40	0.142	0.205
σ_v	No S0's	39	0.080	0.319
a_4	Full	31	0.560	<0.005
a/b, σ_v	Full	41	0.096	0.282
a/b, σ_v	No cE's	40	0.079	0.321
a/b, σ_v	No S0's	39	0.060	0.365
a/b, a_4	Full	31	0.492	<0.005
σ_v, a_4	Full	31	0.044	>0.400
a/b, σ_v, a_4	Full	31	0.016	>0.400

[a] The following combinations show no correlations: a/b-κ_1 and a_4-κ_1.

TABLE A2

PARTIAL SPEARMAN RANK ANALYSIS: TRENDS WITH κ_2

Test Pair[a] and Held Parameters (1)	Sample (2)	Size (3)	Partial Spearman Rank (4)	Probability (5)
L_B-κ_2:				
L_X	Full	44	−0.354	0.011
L_X	No cE's	43	−0.320	0.022
L_X	No S0's	40	−0.331	0.022
L_6	Full	44	−0.358	0.010
L_6	No cE's	43	−0.346	0.015
L_6	No S0's	40	−0.350	0.017
L_X, L_6	Full	44	−0.264	0.048
L_X, L_6	No cE's	43	−0.249	0.062
L_X, L_6	No S0's	40	−0.273	0.050

[a] The following test pairs show no correlation: L_X-κ_2, L_6-κ_2, a/b-κ_2, Mg_2-κ_2, and a_4-κ_2.

TABLE A3

PARTIAL SPEARMAN RANK ANALYSIS: TRENDS WITH κ_3

Test Pair[a] and Held Parameters (1)	Sample (2)	Size (3)	Partial Spearman Rank (4)	Probability (5)
L_B-κ_3:				
L_X	Full	44	0.132	0.208
L_X	No cE's	43	0.097	0.271
L_X	No S0's	40	0.064	0.352
L_6	Full	44	0.225	0.078
L_6	No cE's	43	0.209	0.095
L_6	No S0's	40	0.177	0.152
L_X, L_6	Full	44	0.035	>0.400
L_X, L_6	No cE's	43	0.018	>0.400
L_X, L_6	No S0's	40	−0.017	>0.400
L_X-κ_3:				
L_B	Full	44	0.343	0.014
L_B	No cE's	43	0.336	0.017
L_B	No S0's	40	0.351	0.016
L_6	Full	44	0.379	0.007
L_6	No cE's	43	0.363	0.010
L_6	No S0's	40	0.365	0.013
L_B, L_6	Full	44	0.314	0.023
L_B, L_6	No cE's	43	0.304	0.028
L_B, L_6	No S0's	40	0.325	0.024
a/b-κ_3:				
Mg_2	Full	41	−0.156	0.181
Mg_2	No cE's	40	−0.178	0.150
Mg_2	No S0's	39	−0.164	0.175
σ_v	Full	41	−0.133	0.215
σ_v	No cE's	40	−0.147	0.196
σ_v	No S0's	39	−0.091	0.293
a_4	Full	31	−0.418	0.011
Mg_2, σ_v	Full	41	−0.069	0.341
Mg_2, σ_v	No cE's	40	−0.080	0.318
Mg_2, σ_v	No S0's	39	−0.033	>0.400
Mg_2, a_4	Full	31	−0.259	0.089
σ_v, a_4	Full	31	−0.260	0.088
Mg_2, σ_v, a_4	Full	31	−0.207	0.156
Mg_2-κ_3:				
a/b	Full	41	0.512	<0.005
a/b	No cE's	40	0.464	<0.005
a/b	No S0's	39	0.462	<0.005
σ_v	Full	41	0.278	0.044
σ_v	No cE's	40	0.267	0.052
σ_v	No S0's	39	0.241	0.077
a_4	Full	31	0.627	<0.005
a/b, σ_v	Full	41	0.255	0.062
a/b, σ_v	No cE's	40	0.238	0.079
a/b, σ_v	No S0's	39	0.227	0.092
a/b, a_4	Full	31	0.560	<0.005
σ_v, a_4	Full	31	0.332	0.041
a/b, σ_v, a_4	Full	31	0.294	0.068

[a] The following test pairs show no correlation: L_6-κ_3 and a_4-κ_3.

TABLE A4

PARTIAL SPEARMAN RANK ANALYSIS: TRENDS WITH $\delta\kappa_3$

Test Pair[a] and Held Parameters (1)	Sample (2)	Size (3)	Partial Spearman Rank (4)	Probability (5)
a/b-$\delta\kappa_3$:				
Mg_2	Full	41	−0.121	0.233
Mg_2	No cE's	40	−0.075	0.327
Mg_2	No S0's	39	−0.145	0.202
σ_v	Full	41	−0.157	0.178
σ_v	No cE's	40	−0.120	0.236
σ_v	No S0's	39	−0.186	0.141
a_4	Full	31	−0.467	<0.005
Mg_2, σ_v	Full	41	−0.105	0.263
Mg_2, σ_v	No cE's	40	−0.041	>0.400
Mg_2, σ_v	No S0's	39	−0.114	0.250
Mg_2, a_4	Full	31	−0.339	0.038
σ_v, a_4	Full	31	−0.378	0.022
Mg_2, σ_v, a_4	Full	31	−0.327	0.046
Mg_2-$\delta\kappa_3$:				
a/b	Full	41	0.285	0.040
a/b	No cE's	40	0.385	0.009
a/b	No S0's	39	0.383	0.010
σ_v	Full	41	0.236	0.076
σ_v	No cE's	40	0.302	0.033
σ_v	No S0's	39	0.327	0.024
a_4	Full	31	0.566	<0.005
a/b, σ_v	Full	41	0.205	0.108
a/b, σ_v	No cE's	40	0.282	0.045
a/b, σ_v	No S0's	39	0.294	0.041
a/b, a_4	Full	31	0.480	<0.005
σ_v, a_4	Full	31	0.429	0.010
a/b, σ_v, a_4	Full	31	0.387	0.022
σ_v-$\delta\kappa_3$:				
a/b	Full	41	0.217	0.092
a/b	No cE's	40	0.312	0.028
a/b	No S0's	39	0.279	0.047
Mg_2	Full	41	0.101	0.268
Mg_2	No cE's	40	0.168	0.164
Mg_2	No S0's	39	0.146	0.201
a_4	Full	31	0.421	0.010
a/b, Mg_2	Full	41	0.081	0.313
a/b, Mg_2	No cE's	40	0.157	0.185
a/b, Mg_2	No S0's	39	0.114	0.250
a/b, a_4	Full	31	0.313	0.049
Mg_2, a_4	Full	31	0.109	0.288
a/b, Mg_2, a_4	Full	31	0.058	0.386

[a] The following test pairs show no correlation: L_B-$\delta\kappa_3$, L_X-$\delta\kappa_3$, L_6-$\delta\kappa_3$, and a_4-$\delta\kappa_3$.

REFERENCES

Bender, R., Burstein, D., & Faber, S. M. 1992, ApJ, 399, 462
———. 1993, ApJ, 411, 153
Bender, R., & Surma, P. 1992, A&A, 258, 250
Bender, R., Surma, P., Döbereiner, S., Möllenhoff, C., & Madejesky, R. 1989, A&A, 217, 35
Buzzoni, A., Gariboldi, G., & Mantegazza, L. 1992, AJ, 103, 1814
Carollo, C. M., Danziger, I. J., & Buson, L. 1993, MNRAS, 265, 553
Ciotti, L., D'Ercole, A., Pellegrini, S., & Renzini, A. 1991, ApJ, 376, 380
Davies, R. L., Sadler, E. M., & Peletier, R. F. 1993, MNRAS, 262, 650
Djorgovski, S., & Davis, M. 1987, ApJ, 313, 59
Djorgovski, S., & de Carvalho, R. 1990a, in Ap&SS Conf. Proc. 160, Windows on Galaxies, ed. G. Fabbiano, J. S. Gallagher, & A. Renzini (Dordrecht: Kluwer), 9
———. 1990b, in Ap&SS Conf. Proc. 160, Windows on Galaxies, ed. G. Fabbiano, J. S. Gallagher, & A. Renzini (Dordrecht: Kluwer), 307
Dressler, A., Lynden-Bell, D., Burstein, D., Davies, R. L., Faber, S. M., Terlevich, R. J., & Wegner, G. 1987, ApJ, 313, 42
Eskridge, P. B., Fabbiano, G., & Kim, D-W. 1995a, ApJ, 442, 523 (P2)
———. 1995b, ApJS, 97, 141 (P1)
Fabbiano, G. 1989, ARA&A, 27, 87
Fabbiano, G., Gioia, I. M., & Trinchieri, G. 1988, ApJ, 324, 749
———. 1989, ApJ, 347, 127 (FGT)
Fabbiano, G., Kim, D-W., & Trinchieri, G. 1992, ApJS, 80, 531 (P0)
Fabbiano, G., Kim, D-W., & Trinchieri, G. 1994, ApJ, 429, 94
Feigelson, E. D., & Babu, G. J. 1992, Statistical Challenges in Modern Astronomy (New York: Springer)
Feigelson, E. D., & Nelson, P. I. 1985, ApJ, 293, 192
Forman, W., Jones, C., & Tucker, W. 1985, ApJ, 293, 102
Forman, W., Schwarz, J., Jones, C., Liller, W., & Fabian, A. C. 1979, ApJ, 234, L27
Isobe, T., Feigelson, E. D., & Nelson, P. I. 1986, ApJ, 306, 490
Kendall, M., & Stuart, A. 1976, The Advanced Theory of Statistics, Vol. 2 (New York: Macmillan)
Kim, D.-W., Fabbiano, G., & Trinchieri, G. 1992, ApJ, 393, 134
Kormendy, J. 1985, ApJ, 295, 73
Lauer, T. R. 1985, ApJ, 292, 104
LaValley, M. P., Isobe, T., & Feigelson, E. D. 1992, BAAS, 24, 839
Schmitt, J. H. M. M. 1985, ApJ, 293, 178
Trinchieri, G., & Fabbiano, G. 1985, ApJ, 296, 447
Vader, J. P. 1986, ApJ, 306, 390
Woosley, S. E., & Weaver, T. A. 1986, in IAU Colloq. 89, Radiation Hydrodynamics in Stars & Compact Objects, ed. D. Mihalas & K. H. Winkler (Berlin: Springer), 91
Worthey, G. 1993, ApJ, 409, 530
Worthey, G., Faber, S. M., & Gonzalez, J. J. 1992, ApJ, 398, 69